

Article

Influence of Magnesium Aluminate Nanoparticles on Epoxy-Based Intumescent Flame Retardation Coating System

Hatem Abuhimd ^{1,*},[†], Tentu Nageswara Rao ^{2,†}, Jung-il Song ³, Prashanthi Yarasani ⁴, Faheem Ahmed ^{5,*}, Botsa Parvatamma ⁶, Asma A. Alothman ⁷, Murefah Mana AL-Anazy ⁸ and Ahmad A. Ifseisi ⁷

¹ National Nanotechnology Center, King Abdulaziz City for Science and Technology, P.O. Box 6086, Riyadh 11442, Saudi Arabia

² Department of Chemistry, Krishna University, Machilipatnam, Andhra Pradesh 521001, India; tnraochemistry@gmail.com

³ Department of Mechanical Engineering, Changwon National University, Changwon 51140, Korea; jisong@changwon.ac.kr

⁴ Department of Chemistry, Mahatma Gandhi University, Nalgonda, Telangana 508254, India; dryprasanthi@gmail.com

⁵ Department of Physics, College of Science, King Faisal University, Hofuf, Al-Ahsa 31982, Saudi Arabia

⁶ Department of Organic Chemistry, Gayathri P.G Courses, Gotlam, Vizianagaram 535003, India; Parvathi1787@rediffmail.com

⁷ Chemistry Department, College of Science, King Saudi University, Riyadh 11451, Saudi Arabia; aalothman@ksu.edu.sa (A.A.A.); aifseisi@ksu.edu.sa (A.A.I.)

⁸ Department of Chemistry, College of Science, Princess Nourah bint Abdulrahman University, Riyadh 11671, Saudi Arabia; mmalanazy@pnu.edu.sa

* Correspondence: abuhimd@gmail.com (H.A.); fahmed@kfu.edu.sa (F.A.)

† These two authors contributed equally.

Received: 17 September 2020; Accepted: 5 October 2020; Published: 12 October 2020



Abstract: Ethylenediamine modified ammonium polyphosphate (EDA-MAPP) and charring-foaming agents (CFA) were prepared using a simple chemical method and further used to make intumescent flame retardant coatings based on epoxy resin. The content of MAPP and CFA was fixed at a ratio of 2:1. Nanoparticles of magnesium aluminate ($MgAl_2O_4$ NPs) have been introduced into the flame retardant coating formulation in various quantities to evaluate the promotional action of $MgAl_2O_4$ NPs with a flame retardant coating system. The promotional action of $MgAl_2O_4$ NPs on the flame retardant coating formulation was studied using a vertical burning test (UL-94V), limiting oxygen index (LOI), thermogravimetric analysis (TGA) and Fourier transform infra-red spectroscopy (FTIR). The UL-94V results indicated that the addition of $MgAl_2O_4$ effectively increased flame retardancy and met the V-0 rating at each concentration. The TGA results revealed that the incorporation of $MgAl_2O_4$ NPs at each concentration effectively increased the thermal stability of the flame retardant coating system. Cone-calorimeter experiments show that $MgAl_2O_4$ NPs effectively decreased peak heat release rate (PHRR) and total heat release (THR). The FTIR results indicated that $MgAl_2O_4$ NPs can react with MAPP and generate a dense char layer that prevents the transfer of oxygen and heat.

Keywords: $MgAl_2O_4$ NPs; intumescent flame retardation coating system; epoxy coatings; UL-94V; cone-calorimeter; TGA

1. Introduction

Wood has been used as a primary structural raw material due to its valuable properties such as complexion, low mass, high strength and high insulation properties. Due to its high flammability, the application of wood for safety purposes in certain fields is limited [1]. Flame retardant coatings have been developed for the protection of materials such as metals, polymers, textiles and wooden structures. Flame retardant coatings are mainly divided into two types: non-intumescent and intumescent coatings. The use of intumescent coatings is preferred over non-intumescent coatings because intumescent coatings form a foam-like structure on a material surface that restricts the flow of heat and oxygen. The practical application of intumescent flame retardant (IFR) coating technology is therefore recognized as effective in reducing fire damage to wood [2]. In general, the IFR system consists of three main ingredients: an acidic source, a carbonizing agent and a foaming agent [3]. During heating, the IFR coating system can form a protective charred layer to protect the wood substrate from the burning process [4]. The char can be formed by cross-linking and the cyclic reaction of flame retardant molecules [5]. This charred layer slows down the transfer of heat and oxygen between the substrate and its surroundings [6].

Previous studies have shown that the combination of ammonium polyphosphate (APP) and pentaerythritol (PER) has shown effective flame retardation intumescence [7–9]. Other studies also reported that APP, PER and melamine were used in the composition of the IFR system [10]. PER acts as a source of carbonization, but in nature, it is sensitive to moisture. So the water content can easily be absorbed from the atmosphere and oozed out of the IFR system, leading to terrible corrosion. Several studies have been done to develop and apply different types of carbonizing agents in practice [11]. In this regard, researchers have shown a great deal of attention over the last decade to the synthesizing of highly stable charring-foaming agents with triazine derivatives [12]. Triazine derivative acts as a charring agent and also as a foaming agent because it contains abundant amounts of carbon and nitrogen atoms in its structure [13,14]. Various types of triazine derivatives have been used as charring and foaming agents in IFR systems, and their effects have been extensively investigated [15,16]. Many studies in which APP and triazine derivatives have been used as an intumescent flame retardant system have been reported [17–21]. However, there is some limitation because triazine derivatives produce a char that shows poor efficiency [22–24]. To improve char thickness and hardness of promotional agents needs to be incorporated into the IFR system [25–27]. Some studies have utilized promotional agents such as zeolites [28], organoboron siloxanes [29] and some metal compounds and transition metal oxides. These studies have shown that promotional agents can greatly improve the thickness of the char by forming cross-linkages [30,31]. Magnesium aluminate (a white colored powder), is a non-carcinogenic agent. It can be used as a synergist to enhance the performance of an intumescent flame retardant system. It is very cheap and environmentally friendly. It acts as a flame retardant during the condensation phase. It can react with hydroxyl groups of the ammonium polyphosphate resulting in endothermic decomposition.

In this study, the readily available, cost-effective and non-hazardous nanoparticles of magnesium aluminate (MgAl_2O_4 NPs) have been selected as a promotional agent to investigate their action on the epoxy/IFR coating system. The IFR system consists of a modified ammonium polyphosphate ethylenediamine and charring foaming agent (CFA). In this work, the APP is modified with ethylenediamine because APP acts as an acid source and a blowing agent, while MAPP can also show charring action. The CFA polymer was made from a triazine molecule. It is hydrophobic and has a thermally stable triazine ring. Due to these properties, CFA cannot be affected by atmospheric moisture and has a high flame retardant effect. A new IFR coating composition of MAPP and CFA has been prepared to improve the thermal stability and flame retardant performance of a coating composition. An eco-friendly promotional agent, MgAl_2O_4 , is added to this coating composition to increase the thickness of the intumescent char.

The vertical burning test (UL-94V), limiting oxygen index (LOI), Fourier transform infrared spectroscopy (FTIR), thermogravimetric analysis (TGA) and cone calorimeter studies have been employed to investigate the synergism between magnesium aluminate and epoxy/IFR systems.

2. Experimental

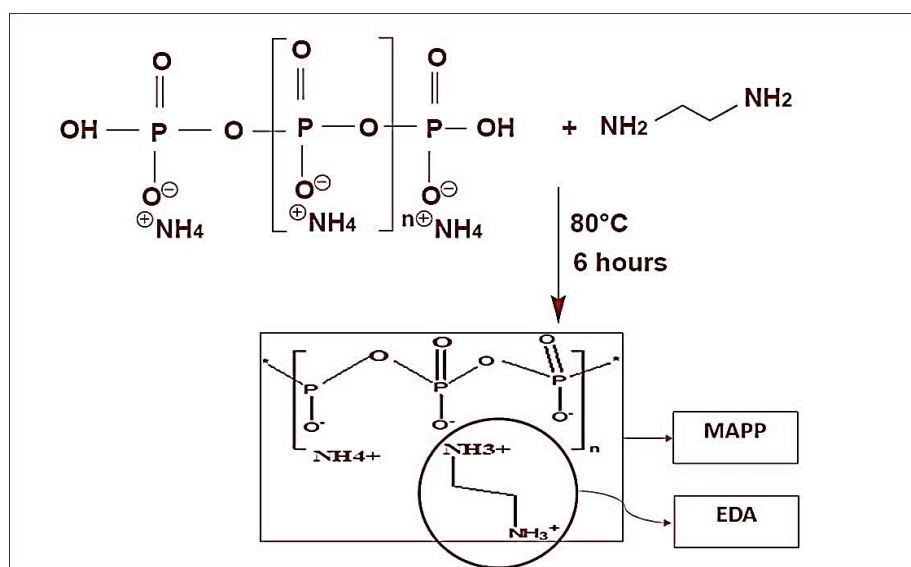
2.1. Materials

The epoxy resin and amine hardener used in this study were obtained from Sigma Aldrich (St. Louis, MO, USA). Ammonium polyphosphate (APP, Crystalline form II, $n \geq 1000$) and ethanol (95% pure) were obtained from Samchun pure chemicals, Pyungtaek, Korea. Ethylenediamine (EDA; 99.5% pure), acetone (99% pure) and ethanolamine (ETA; 99% pure) were analytical grade and obtained from Sigma Aldrich. Cyanuric chloride (99% pure) was procured from Sigma Aldrich. Aluminum isopropoxide, magnesium ethoxide, methanol and isopropanol were supplied by Merck Limited (Kenilworth, NJ, USA). All the solvents and chemicals were used as received.

2.2. Methods

2.2.1. Preparation of MAPP

A mixer of ethanol and water (400 mL:15 mL) was poured into a clean and dry 1000 mL bottom three-necked, a round-bottomed flask which is equipped with a magnetic stirrer. Thirty minutes later, 9 g of ethylenediamine was poured into the flask and stirred at 200 rpm for 20 min. Then, 50 g of APP was slowly added to the above solution. After that, the solution was heated up to 80 °C for 6 h. After the completion of the reaction, the obtained mixture was cooled to room temperature. Then, the resulted white solid was filtered and washed with ethanol and water. The obtained white solids were kept in a hot air oven at 50 °C for 20 h to remove moisture content. The schematic illustration of a chemical reaction is shown (Scheme 1).



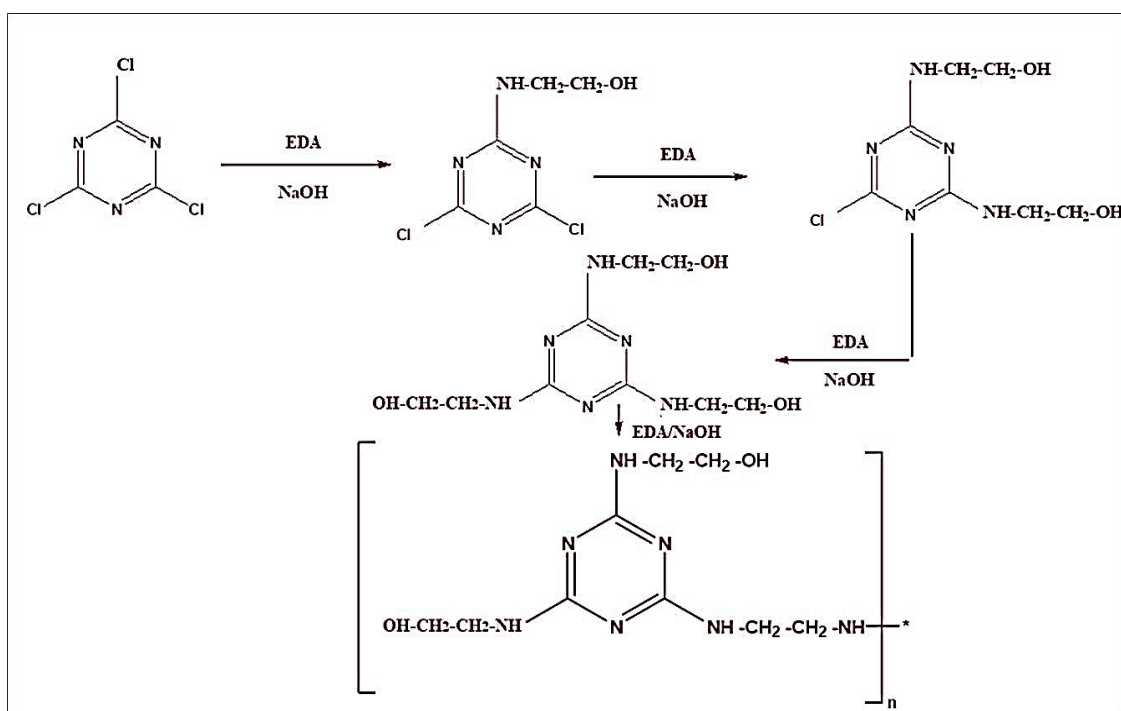
Scheme 1. Reaction between APP and EDA.

2.2.2. Preparation of CFA

The derivative of the triazine-containing macromolecule, which is designated as a charring-foaming agent (CFA) was synthesized via bimolecular nucleophilic substitution (SN^2) reaction mechanism. Initially, 1 mol of cyanuric chloride and 500 mL of acetone were poured into a clean three-neck 2 L flask equipped with a magnetic stirrer that was immersed in an ice-water bath. Then, 1 mol of ethanolamine

and 1 mol of NaOH were completely dissolved in distilled water, and this mixture was slowly added to the flask for a period of 2 h. This step was maintained at 0–10 °C for 4 h. In the first step, 0.5 mol of ethylenediamine and 1 mol of NaOH were dissolved in distilled water and this aqueous solution was added dropwise to the above reaction mixture. Then, the reaction temperature was increased to 50–60 °C. This reaction was continued and proceeded for 4 h.

In the second step of the chemical reaction, a mixture of 0.5 mol of ethylenediamine and 1 mol of NaOH was again dissolved in distilled water; this aqueous solution was added slowly into the reaction flask. Then, the reaction temperature was increased to 75 °C to evaporate acetone solvent. This step was allowed to proceed for 4 h. When the reaction was completed; the obtained mixture was cooled to room temperature and filtered. After filtration, the collected white solid particles were washed with distilled water and dried in a hot air oven at 60 °C for 3 h. The schematic illustration of a chemical reaction is shown (Scheme 2).



Scheme 2. Preparation of charring-foaming agent (CFA).

2.2.3. Synthesis of MgAl₂O₄ NPs

MgAl₂O₄ NPs were synthesized through the hydrolysis reaction using high purity aluminum isopropoxide and magnesium ethoxide raw materials. Initially, 6.2 g of aluminum isopropoxide was dissolved in 1540 mL of isopropanol and 12.5 g of magnesium ethoxide was dissolved in 550 mL of methanol thereby making two distinct solutions. The two solutions were then, combined in a 5 L beaker. The mixed solution was heated at 70 °C for 2 h, followed by adding 330 mL of water and stirring at 200 rpm. The solution was finally filtered and the precipitate obtained was dried at 120 °C for 24 h.

2.2.4. Formulation Sample Preparation

The intumescent flame retardant (IFR) coating system consisted of MAPP, CFA and MgAl₂O₄ NPs as synergists. The ratio of MAPP to CFA was set at 2:1 and the inclusion of MgAl₂O₄ NPs ranged from 0 to 4 wt % respectively. Intumescent flame retardant coating formulations are shown in Table 1. All components were homogeneously mixed using a high-speed dispersion mixer for the preparation of IFR coating formulations. Prepared coatings were applied to specific plywood

pieces with a paint-brush at room temperature. This process was repeated with a coating thickness of 5 ± 2 mm.

Table 1. Composition of the intumescent flame retardation coatings.

Sample	Resin (%)	MAPP (%)	CFA (%)	MgAl ₂ O ₄ NPs
Pure Epoxy Resin	100	0	0	0
Epoxy/IFR	70	20	10	0
Epoxy/IFR/MgAl ₂ O ₄ NPs-2%	68	20	10	2
Epoxy/IFR/MgAl ₂ O ₄ NPs-4%	66	20	10	4

2.2.5. Characterization MgAl₂O₄ NPs

The room temperature XRD profile of the synthesized MgAl₂O₄ NPs was obtained using the “Debye–Scherrer” equation for the crystal structure and sample phase purity and the crystallite size was determined from the XRD spectra. FE-SEM characterization of MgAl₂O₄ NPs (TESCAN, CZ/MIRA I LMH, Brno, Czechia) showed MgO’s production on the Al₂O₃ matrix. The energy dispersive X-ray analysis (EDX) was used for the elemental composition of MgAl₂O₄ NPs. The particle size was found to be 4–5 nm by HRTEM. The FTIR (PerkinElmer, Waltham, MA, USA) was used for the identification of functional groups.

2.2.6. Characterization Methods for Coatings

FTIR Test

A 360 spectrometer instrument (Nicolet Aviator, Nicolet, USA) was used for FTIR analysis in the range of 4000–500 cm⁻¹. For the FTIR analysis, the samples were pressed into pellet forms with KBr powder.

X-ray Diffraction Study

The XRD study was conducted by a D8 X-ray diffractometer model with Cu K α radiation for the structural analysis of samples. The scanning rate of 0.02° per second with the 2° and the scanning range was 5–50°.

Flame Retardancy Test

The LOI values of all coating formulations were measured according to the ASTM-D2863 standard [32] procedure on the HC-2C oxygen index instrument. The coating formulations were applied on plywood sheets of 130 mm \times 6.5 mm \times 3 mm dimension to perform the LOI test. The prepared intumescent flame retardant coatings were applied on the surfaces of all sides of the plywood pieces with dimensions of 127 mm \times 27 mm \times 3 mm. Then, the coated plywood pieces were dried at room temperature for two days. The UL-94V test was performed according to the ASTM-D3801 standard method. The coated plywood sheets were ignited for 30 s to calculate the burning rate, and burning times of each sample.

Thermogravimetric Analysis Test

Thermal stability of all coating formulations was performed using the SDT Q600 V20.9 Build-20 instrument with 20 °C/min heating rate at a temperature range of 30–800 °C under a nitrogen atmosphere at the flow rate of 20 mL/min. The weight of each coating formulation was taken and was approximately 4–5 mg.

Combustion Test

The combustion parameters of all coating formulations were performed on the cone calorimeter following the ISO 5660-2002 standard [33] method by exposing 50 kW m^{-2} of external heat flux. All samples were laid vertically on the sample holder.

3. Result and Discussion

3.1. FTIR of MAPP

Figure 1 shows the FTIR spectra of MAPP and APP. The peak attributed at 3407 cm^{-1} is due to the NH_4^+ ion asymmetric stretching vibrations. From this data, it can be seen that the MAPP spectrum contains peaks at 2916, 2855 and 1536 cm^{-1} , which is specifically attributed to the characteristic stretching absorption peaks of $-\text{CH}_2-\text{CH}_2-$ and NH_3^+ ions. The peaks which appeared correspond to $-\text{CH}_2-\text{CH}_2-$ and NH_3^+ ions in MAPP proved that $\text{NH}_3^{(+)(-)}\text{O}-\text{P}$ bond is formed successfully.

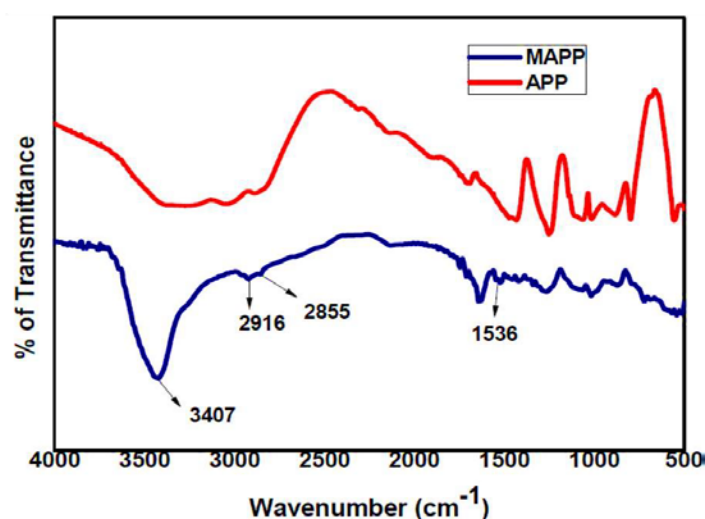


Figure 1. FTIR spectra of APP and MAPP.

3.2. XRD of MAPP

Figure 2 shows the XRD spectra of APP and MAPP. The diffraction peaks of APP and MAPP have appeared in the same position, but a new peak at 11.92° is obtained for MAPP. This specific peak in MAPP is attributed to the presence of $(\text{NH}_4)_5\text{P}_3\text{O}_{10} \cdot \text{H}_2\text{O}$. This result indicated that the crystalline structures of APP are not changed by the reaction between APP and ethylenediamine.

3.3. Thermogravimetric Analysis of CFA

The thermogravimetric analysis can be used to evaluate the loss of mass of the sample with respect to temperature and to provide information on the formation of char, degradation behavior and thermal stability of the sample. The TGA and DTG curves of the CFA are represented in Figures 4 and 5. The CFA has shown that a great amount of char at 800°C was found at 35.90%. This result indicates that the synthesized CFA is a thermally more stable and admirable charring-foaming agent at high temperatures due to its stable triazine ring structure. From the DTG curve, it can be seen that the CFA decomposition has three main steps. The first step takes place in the range of $250\text{--}310^\circ\text{C}$ and the peak at 287°C is due to the evaporation of ammonia and nitrogen gas from the CFA. The second degradation range appears in the range from $310\text{--}370^\circ\text{C}$, this has a peak at 353°C and it is attributed to the partial bond breakage. The third step of decomposition occurs in the $370\text{--}432^\circ\text{C}$ temperature range. In this step, the weight loss has occurred due to the thermal macromolecular backbone structure decomposition.

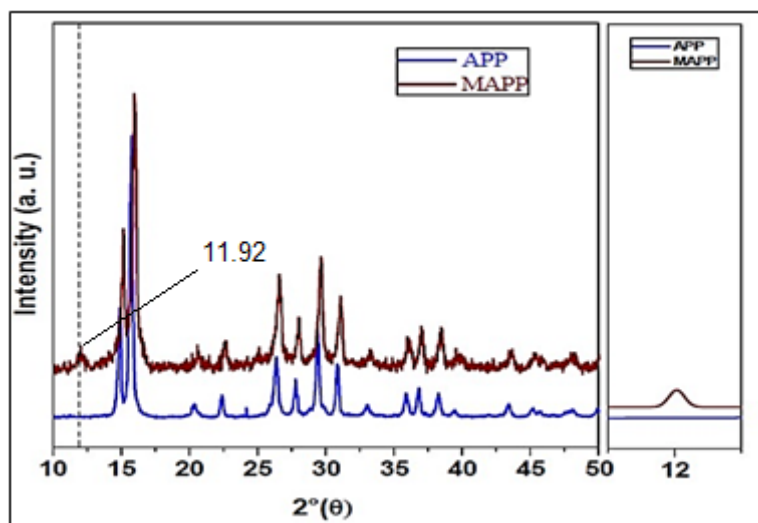


Figure 2. The XRD curves of APP and MAPP.

3.4. FTIR of CFA

The FTIR spectrum of CFA is shown in Figure 3. This spectrum consisting of the broad adsorption peaks in the range of $3300\text{--}3450\text{ cm}^{-1}$ is due to the symmetrical stretching vibrations of N–H and O–H bonds; and the peaks at 2927 and 2850 cm^{-1} can be assigned to $\nu_{\text{C-H}}$ in $-\text{CH}_2-\text{CH}_2-$ group. The peaks at 1580 , 1358 , 1159 and 1060 cm^{-1} can be assigned to the ν_{tr} , $\nu_{\text{tr-N}}$, $\nu_{\text{C-N}}$ and $\nu_{\text{C-O}}$, respectively. Moreover, this spectrum does not show the peak at 850 cm^{-1} which is corresponding to the C–Cl stretching vibration and this indicates that the CFA is formed successfully.

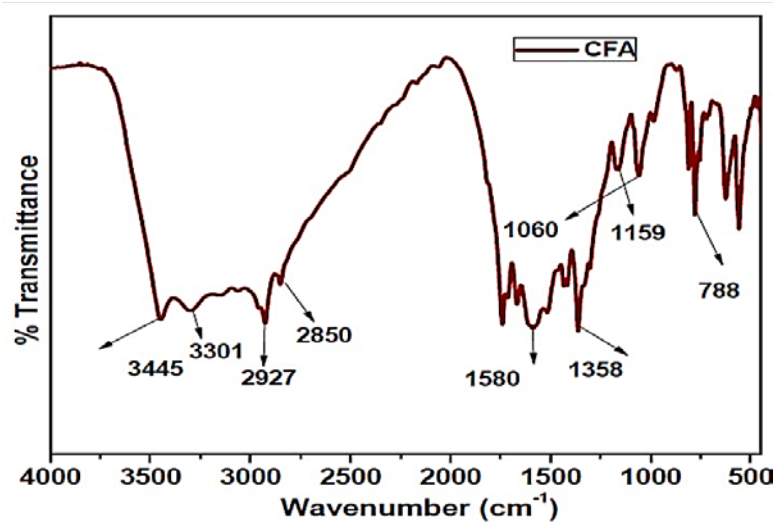


Figure 3. FTIR curve of CFA.

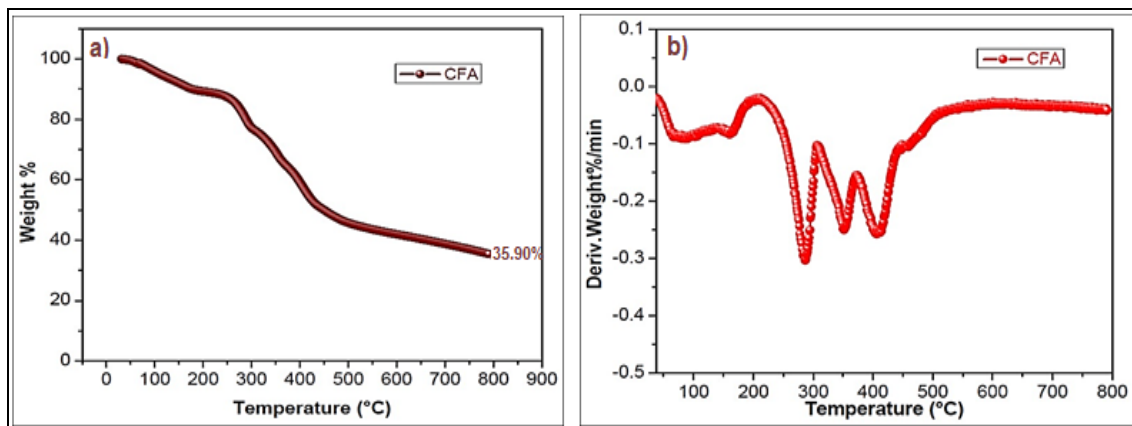


Figure 4. CFA curves (a) thermogravimetric analysis TGA and (b) DTG.

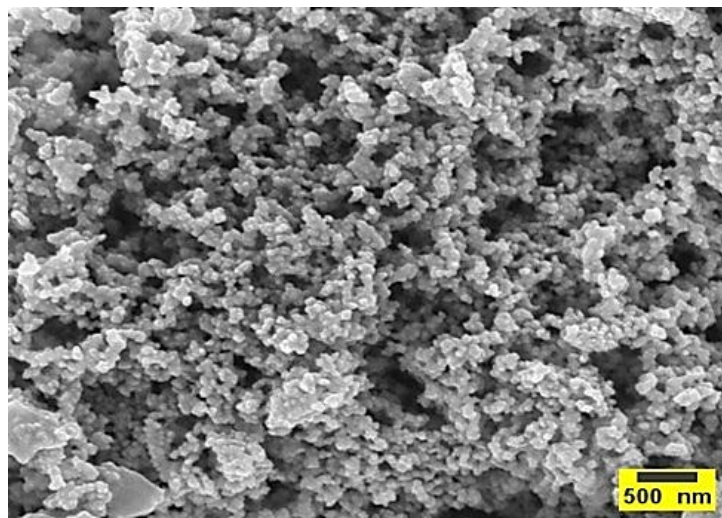


Figure 5. FE-SEM image of MgAl_2O_4 NPs.

3.5. Characterization of MgAl_2O_4 NPs

MgAl_2O_4 NPs synthesized through the hydrolysis reaction were found to possess the average particle size of 5 nm by HRTEM (Figure 5). While the FE-SEM micrograph revealed the presence of particles with irregular shapes and sizes (Figure 6). Furthermore, in some regions, the interconnectivity of the particles has increased which has given rise to agglomerated regions within the sample. Thus, it is speculated here that some particles within the sample act as nucleation centers around which condensation of the smaller particles occurs and hence gives rise to agglomeration [34].

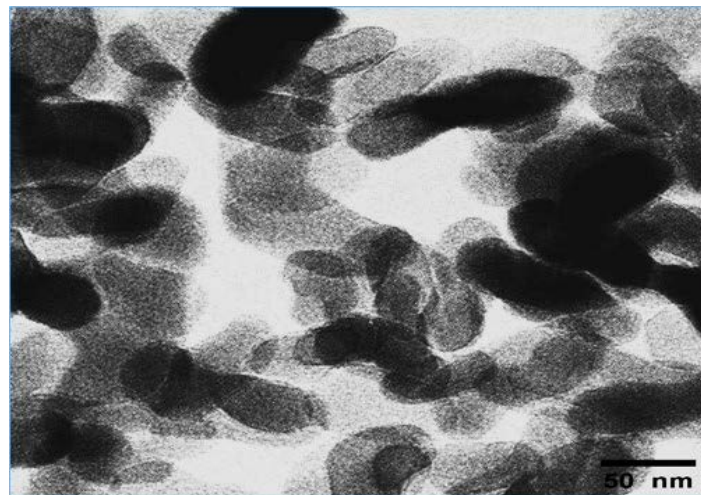


Figure 6. HRTEM micrograph of MgAl₂O₄ NPs.

The room temperature XRD profile for the MgAl₂O₄ synthesized sample is shown in Figure 7. The XRD profile clearly showed the formation of the cubic spinel phase in the fabricated sample. The lattice parameter for the cubic structure was obtained from the XRD pattern using powder-x software. Further, no impurity peak was observed in the complete XRD pattern confirming the formation of the phase pure material.

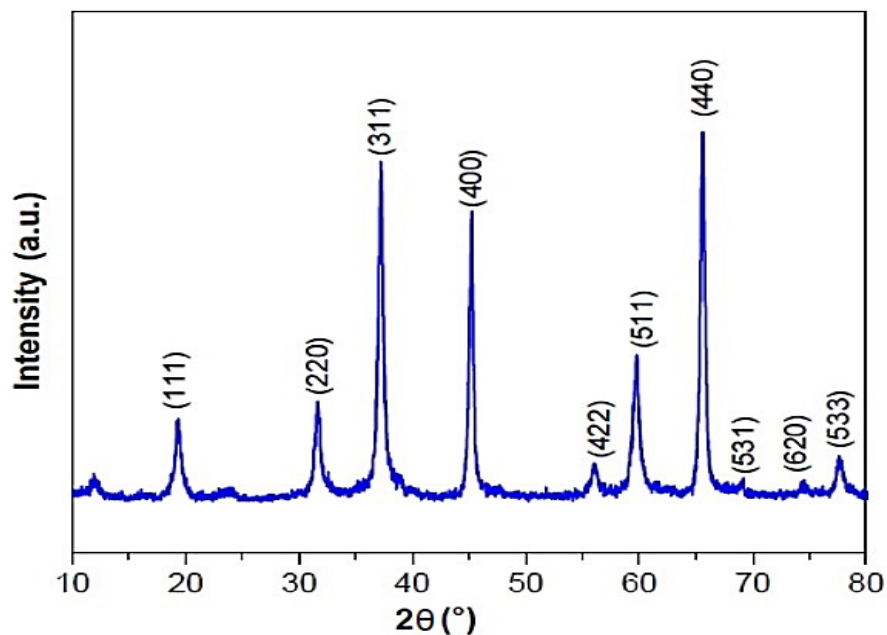


Figure 7. XRD pattern of MgAl₂O₄ NPs.

The FTIR spectrum revealed the band at 522 cm⁻¹ related to Al–O stretching vibration that corresponds to the AlO₆ groups that build up the MgAl₂O₄ composition (Figure 8). The strong absorption at 3438 cm⁻¹ is the stretching vibration of hydroxyl (OH) and a peak at 1644 cm⁻¹ is due to the bending vibration of the adsorbed water molecule [35]. The major peak at 708 cm⁻¹ shows the presence of Mg–O vibrations. The weak band at 1411 cm⁻¹ provides the presence of organic content due to C–O stretching vibration.

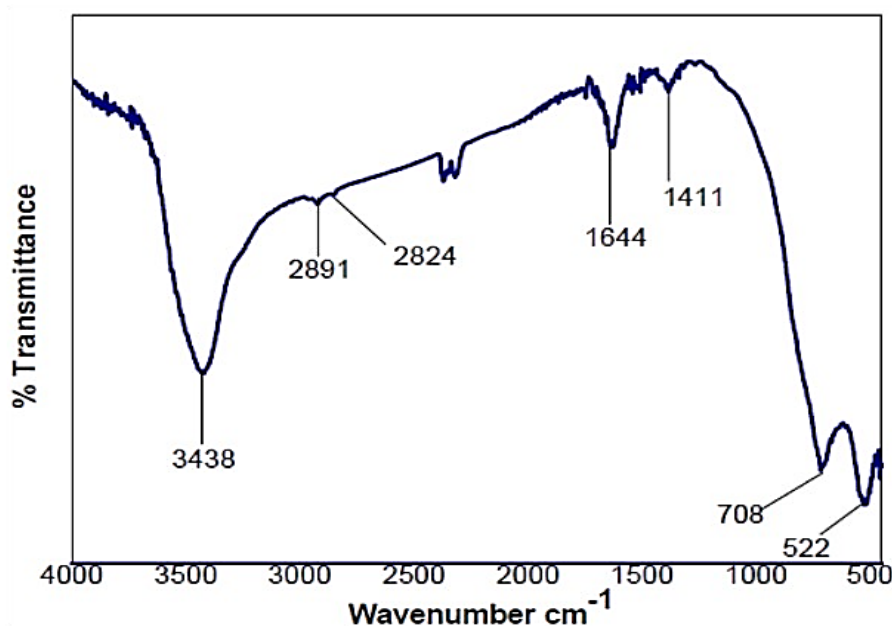


Figure 8. FTIR spectra of MgAl₂O₄ NPs.

The elemental composition of MgAl₂O₄ NPs was studied by EDS as shown in Figure 9. The MgAl₂O₄ NPs exhibit three elemental peaks, one for magnesium element located at 1.1 keV, one for oxygen element located at 0.5 keV and aluminum element located at 1.5 keV. From EDS data, the weight ratio of Mg:Al:O is around 16.39:34.59:49.03. The sample consists of only “O”, “Mg” and “Al” elements.

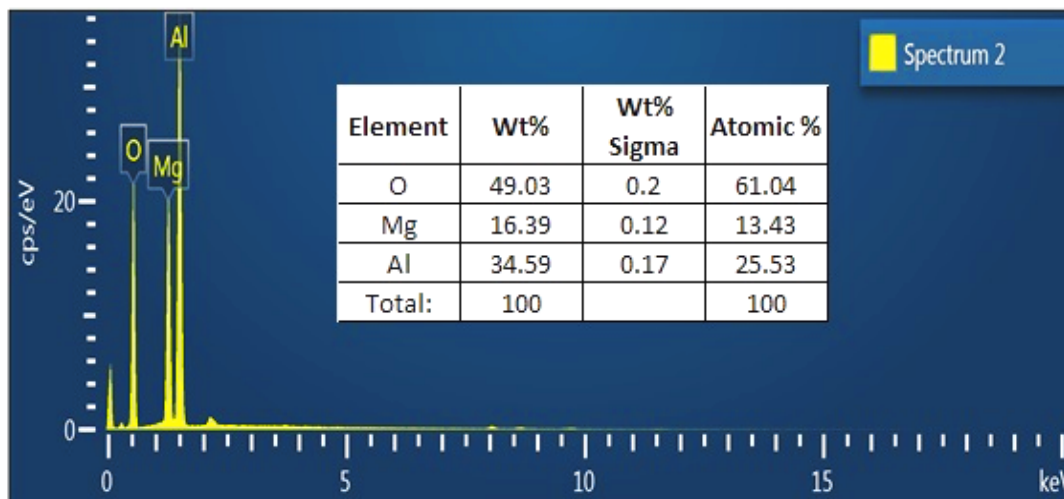


Figure 9. EDS of MgAl₂O₄ NPs.

3.6. Flame Retardancy Test

Table 2 represents the LOI values of the epoxy/IFR systems with a varied ratio of MAPP and CFA. The data clearly shows that by increasing the addition of MAPP, the LOI values first remarkably increased, then, gradually decreased. When the ratio of MAPP and CFA is 2:1, it reached a maximum value at 31.2 and this one passes the burning test with a V-0 rating. A condensation reaction takes place between MAPP and CFA to form a dense, protective char layer which can inhibit the flow of oxygen and heat in between burning material and its surroundings. In the case of a lesser content of MAPP, a crumbled charred layer is formed which is ineffective to restrict the flow of oxygen and heat. On the other hand, when the amount of MAPP reached the maximum level, then it could produce

an excess amount of gasses like ammonia and nitrogen which resulted in the broken of the stable charred layer. Hence, the combination of MAPP and CFA has shown effective action at the optimal ratio of 2:1.

Table 2. Limiting oxygen index (LOI) and a vertical burning test (UL-94V) results of the coatings.

Sample	LOI (%)	UL-94V
Pure Epoxy Resin	25.2	No rating
Epoxy/IFR	31.2	V-0
Epoxy/IFR/MgAl ₂ O ₄ NPs-2%	31.9	V-0
Epoxy/IFR/MgAl ₂ O ₄ NPs-4%	32.6	V-0
STDEV	3.40	

Table 2 represents the LOI values and UL-94V ratings of the epoxy/IFR and epoxy/IFR/MgAl₂O₄ NPs coating systems. The data reveals that the addition of MgAl₂O₄ NPs effectively increases the LOI value of the epoxy/IFR system. The addition of MgAl₂O₄ NPs at 2 wt %, 4 wt %, remarkably increased the LOI values from 31.2 to 31.9 and 32.6, respectively. The reason behind increasing the LOI values is that MgAl₂O₄ NPs can be involved in a chemical reaction with the IFR system. In addition to this, MgAl₂O₄ NPs can also act as catalysts for the condensation reaction between MAPP and CFA. From Table 2 data, it can be seen that epoxy/IFR and epoxy/IFR/MgAl₂O₄ NPs systems pass the UL-94V test and can reach a V-0 rating. The IFR system forms the intumescent char on burning which is responsible for slowing down the burning process and finally results in the extinguishing of the fire. Thus, all the coating formulations would reach a V-0 rating.

3.7. Thermogravimetric Analysis of Coatings

Figures 10 and 11, and Table 3 show the TGA results of the IFR coatings with different amounts of MgAl₂O₄ NPs under the nitrogen atmosphere. In comparison, the TGA curves of the epoxy/IFR/MgAl₂O₄ NPs-2% and epoxy/IFR/MgAl₂O₄ NPs-4% are showing high thermal stability. From the data, it can be seen that the pure resin decomposes at 192 °C (5% T_{onset}) with a maximum temperature of 359 °C where it has 15.5 MLR%/min. Pure resin coating has shown 6.6% char residue at above 500 °C and it is burnt up to 93.5%. The T_{onset} 5% temperature of pure epoxy, epoxy/IFR, epoxy/IFR/MgAl₂O₄ NPs-2% and epoxy/IFR/MgAl₂O₄ NPs-4% coatings are 192, 187, 165 and 122 °C, respectively. The char residue percentage at 800 °C of the epoxy, epoxy/IFR, epoxy/IFR/MgAl₂O₄ NPs-2% and epoxy/IFR/MgAl₂O₄ NPs-4% coatings are 6.6%, 18.5%, 23.7% and 27.5% with MLR%/min values of 15.2, 12.3, 11.1 and 8.3, respectively. From this data, it can be observed that epoxy/IFR is more thermally stable than pure epoxy coating because during burning MAPP and CFA it undergoes an esterification reaction to form a char which protects the flow of heat and oxygen to the coating material, therefore, it will be more stable. The Table 3 data indicates that epoxy/IFR/MgAl₂O₄ NPs-2% and epoxy/IFR/MgAl₂O₄ NPs-4% coatings have lower thermal initial decomposition temperatures, lower MLR%/min and high char residue percentages, due to that the MgAl₂O₄ NPs can catalyze the esterification reaction between MAPP and CFA to form a thick protective char layer [36]. This CFA is gently involved in the esterification reaction because it is a polyhydroxy triazine polymer. From this data, it is clear that the addition of MgAl₂O₄ NPs can increase the thermal stability of the coating formulations.

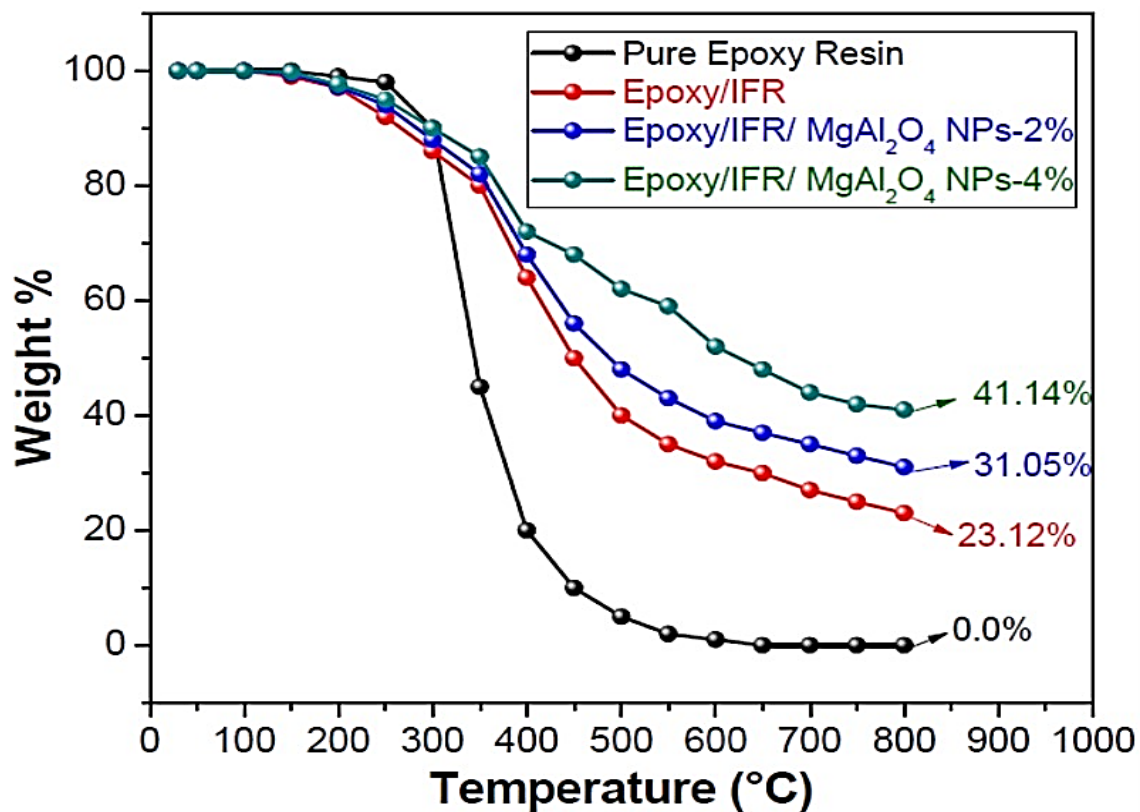


Figure 10. TGA curves of coatings.

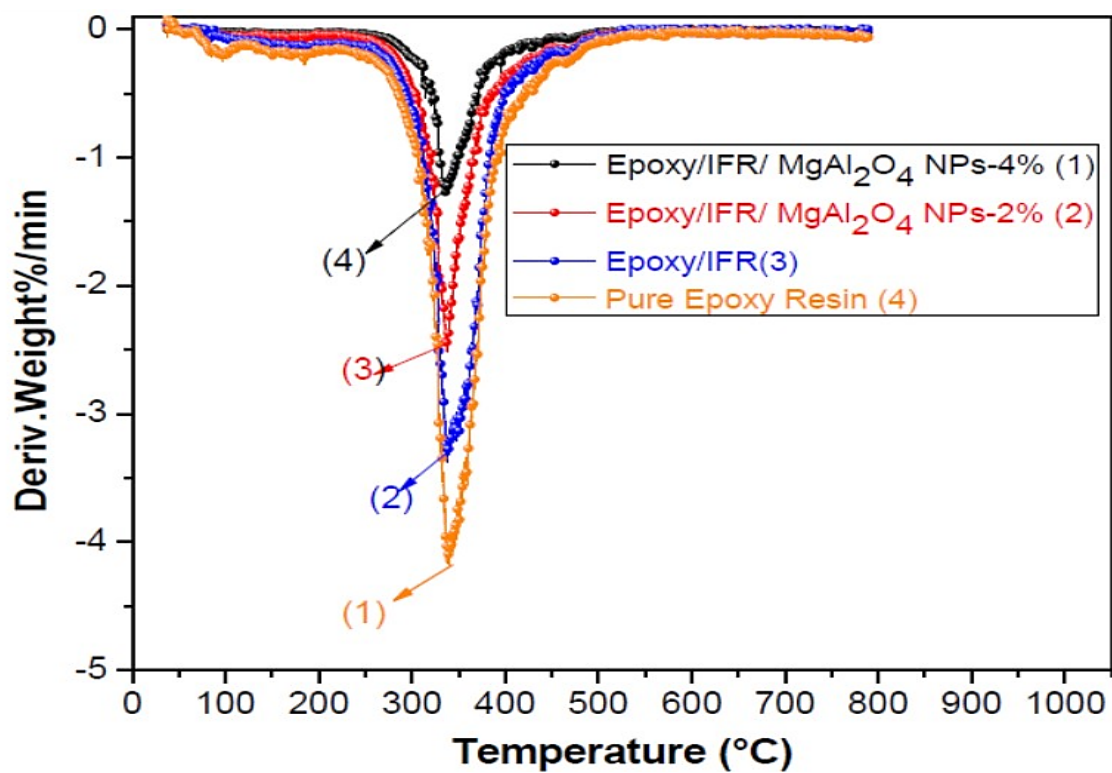


Figure 11. DTG curves of coatings.

Table 3. Thermogravimetric results of the coatings under nitrogen atmosphere.

Sample	T_{onset} (°C)	MLR%/min	Char Residue (%) at 800 °C
Pure Epoxy Resin	192	15.2	0.00
Epoxy/IFR	187	12.3	23.12
Epoxy/IFR/MgAl ₂ O ₄ NPs-2%	165	11.2	31.05
Epoxy/IFR/MgAl ₂ O ₄ NPs-4%	122	8.3	41.14

3.8. Cone-Calorimetric Analysis

The combustion study of a sample can be performed by a cone-calorimeter based on the oxygen consumption principle. Cone calorimetric analysis provides the information for time to ignition (TTI), peak heat release rate (PHRR), total heat release (THR) and total smoke production (TSP). The PHRR values are regarded as an important indicator to characterize the flammability of material in a fire situation. The PHRR curves of all coating compositions are shown in Figure 12 and Table 4. As shown in Figure 13 and Table 4 [34], the pure epoxy coating has shown a single and sharp HRR peak with 756 kW/m² at 177 s whereas the epoxy/IFR, epoxy/IFR/MgAl₂O₄ NPs-2 wt %, and epoxy/IFR/MgAl₂O₄ NPs-4 wt %, coatings have PHRR peaks at 260, 207 and 97.8 kW/m², respectively. When the IFR and MgAl₂O₄ NPs are introduced into the coatings, a great decrease in PHRR values is observed. It is due to that during the combustion process, the IFR system and MgAl₂O₄ NPs is involved in the formation of a dense char layer, which inhibits the flow of oxygen and heat to the material, thus lowering the intensity of the pyrolysis process and also decreases the heat release rate.

From the Figure 10 and Table 4 data, it can be seen that epoxy/IFR, epoxy/IFR/MgAl₂O₄ NPs-2 wt % and epoxy/IFR/MgAl₂O₄ NPs-4 wt % coatings have shortened the ignition time which is significantly attributed to the formation of the protective char layer. At the initial stage of burning, the temperature of these coatings rises gently due to the char formation; therefore it results in a shortening of ignition time. The MgAl₂O₄ NPs play a remarkable role in improving the strength of the char layer, protection of the char from damage and cracking to achieve low HRR values.

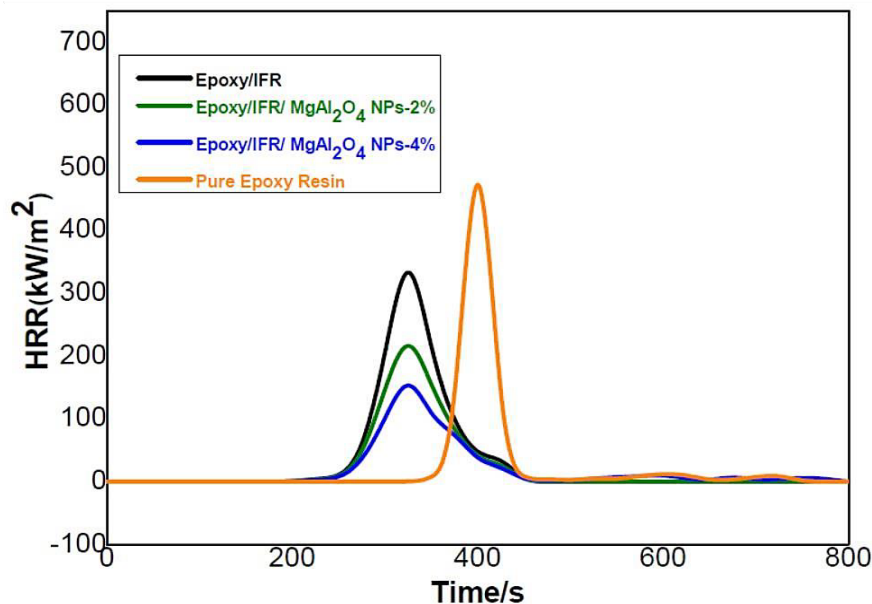
**Figure 12.** PHRR curves of coatings.

Table 4. Cone calorimeter results of the coatings.

Sample	TTI (S)	PHRR (kW m^{-2})	THR ($\text{MJ m}^{-2} \text{kg}^{-1}$)
Pure Epoxy Resin	60	453	82
Epoxy/IFR	55	321	63
Epoxy/IFR/MgAl ₂ O ₄ NPs-2%	43	203	42
Epoxy/IFR/MgAl ₂ O ₄ NPs-4%	43	105	25

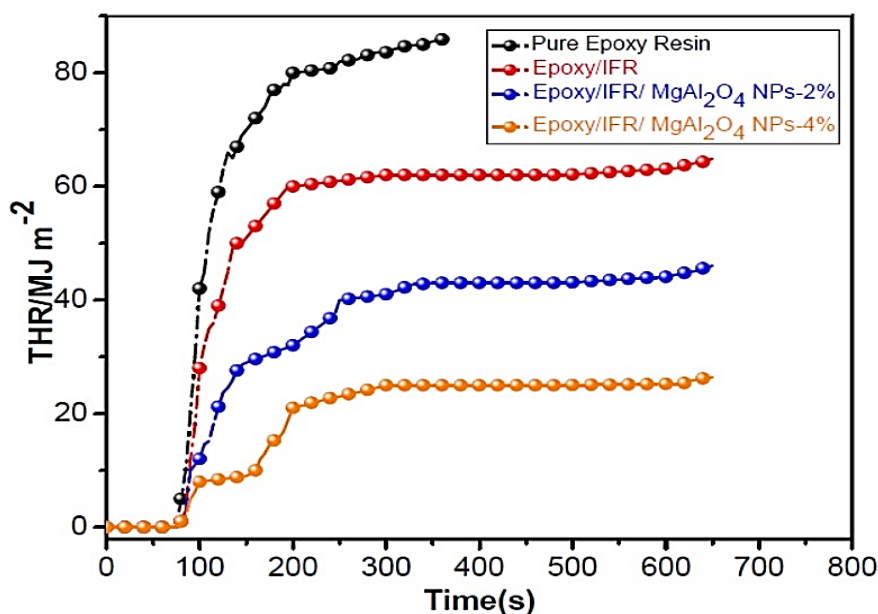


Figure 13. THR curves of coatings.

The THR values of all coatings are shown in Figure 12 and Table 4. From the data, the difference in pure epoxy coating and epoxy/IFR, epoxy/IFR/MgAl₂O₄ NPs-2 wt % and epoxy/IFR/MgAl₂O₄ NPs-4 wt % coatings are seen after 50 s. The THR value of epoxy is 82 MJ/m² at 300 s whereas the THR value of epoxy/IFR, epoxy/IFR/MgAl₂O₄ NPs-2 wt %, and epoxy/IFR/MgAl₂O₄ NPs-4 wt %, is 63 MJ/m², 42 MJ/m² and 24 MJ/m², respectively. These results indicate that the addition of IFR and MgAl₂O₄ NPs greatly decreases the heat release rate. It is due to the MAPP and CFA agents forming a dense protective char layer in the presence of MgAl₂O₄ NPs' promotional agents. The formed char layer lowers the heat released from the material.

From this data, it is proved that MgAl₂O₄ NPs enhance the thickness and strength of the char layer and improves the combustion properties of the coatings.

3.9. Compositions of Charred Layers

Previous studies reveal that upon burning, the intumescent flame retardant system forms a protective charred layer on the surface of the material. The charred layer can inhibit the flow of oxygen and heat in between the material and surroundings. The IFR system also releases the non-flammable gases and moisture into the surroundings to dilute the heat and oxygen around the burning material. Consequently, the char layer can stop the burning process and increase the flame resistance of the material. The charred layers of all coating formulations were formed by constant heating in the muffle furnace at 500 °C for 20 min.

Figure 14 shows the FTIR spectrum of the epoxy/IFR, epoxy/IFR/MgAl₂O₄ NPs-2 wt %, and epoxy/IFR/MgAl₂O₄ NPs-4 wt % charred layers. From Figure 14 data, it can be seen that the absorption peaks in the range of 2900–2950 cm⁻¹ correspond to the symmetric and asymmetric stretching vibrations of C-H bonds in the CH₂ group. The increasing intensity order of these peaks is epoxy/IFR ≤ epoxy/IFR/MgAl₂O₄ NPs-2 wt % ≤ epoxy/IFR/MgAl₂O₄ NPs-4 wt %. This order of

absorption peak intensity demonstrates that MgAl_2O_4 NPs can form cross-linkages with the IFR system and effectively protect the material from the fire. The peaks at $920\text{--}1088\text{ cm}^{-1}$ are assigned to the P–O–C, P–O–P and P–O bonds' stretching vibrations in the phospho-carbonaceous complex. These peaks of epoxy/IFR/ MgAl_2O_4 NPs-2 wt % and epoxy/IFR/ MgAl_2O_4 NPs-4 wt % are showing higher intensity and broadness than epoxy/IFR/ MgAl_2O_4 NPs-0 wt %. MgAl_2O_4 NPs are indicators that act as catalysts, and show promotional action on the formation of a dense intumescent phosphor-carbonaceous char. The absorption peak at 642 cm^{-1} is preferentially attributed to the stretching vibration of the Mg–Al–O bond which indicates that MgAl_2O_4 NPs can form cross-linkages with the IFR system. The intensity of this peak increased as the amount of MgAl_2O_4 NPs increased. These results suggested that MgAl_2O_4 NPs can promote the thickness of the char.

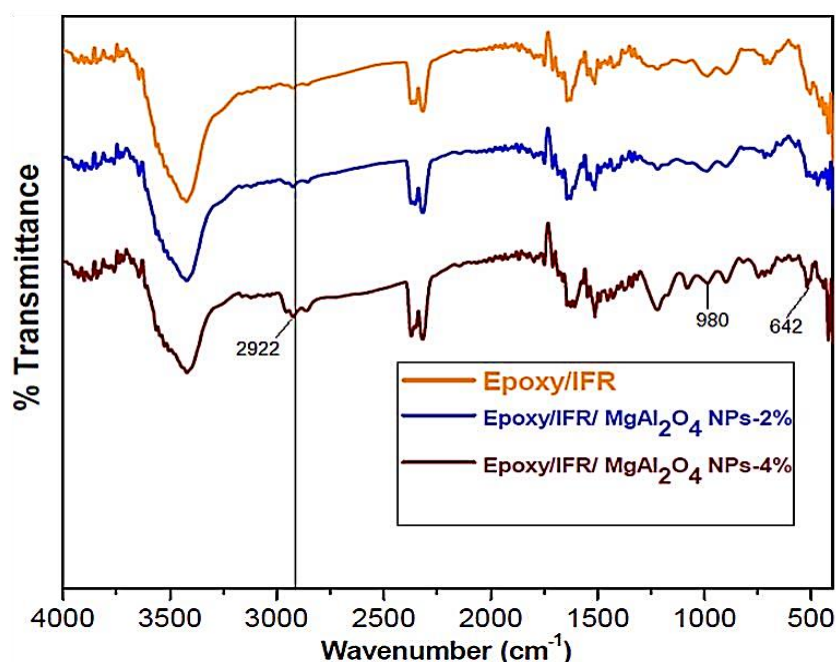


Figure 14. FTIR spectra of epoxy/IFR, epoxy/IFR/ MgAl_2O_4 NPs-2% and epoxy/IFR/ MgAl_2O_4 NPs-4% coatings.

4. Conclusions

Ethylenediamine modified ammonium polyphosphate and N-ethanolamine triazine ethylenediamine copolymer (CFA) are synthesized successfully and their properties were thoroughly investigated and compared. The promotional effect of magnesium aluminate is assessed on the epoxy/IFR coating system. The results of UL-94V and LOI show that MgAl_2O_4 NPs have significantly increased the flame retardancy of the coating system. As the content of MgAl_2O_4 NPs increased in the IFR coating system, the LOI values also increased significantly. From the TGA results, the addition of MgAl_2O_4 NPs significantly increased the thermal stability of the coating system and the interaction between MAPP and MgAl_2O_4 is well demonstrated by FTIR results. The study of the promotional effect of MgAl_2O_4 NPs on the epoxy/IFR coating system revealed the formation of a stable charred protective layer. All the above results conclude that MgAl_2O_4 NPs are a very effective promotional agent in the epoxy/IFR coating systems.

Author Contributions: Conceptualization, H.A. and T.N.R.; methodology, T.N.R.; software, J.-i.S.; validation, F.A., and P.Y.; formal analysis, B.P.; investigation, H.A.; resources, T.N.R.; data curation, A.A.A.; writing—original draft preparation, A.A.I.; writing—review and editing, T.N.R.; visualization, A.A.I.; supervision, F.A.; project administration, F.A.; funding acquisition, M.M.A.-A. All authors have read and agreed to the published version of the manuscript.

Funding: This research was funded by the Deanship of Scientific Research at King Saud University through research group no. RG-1441-433 and the research was funded by the Deanship of Scientific Research at the Princess Nourah bint Abdulrahman University through the Fast-track Research Funding Program.

Acknowledgments: The authors extend their appreciation to the Deanship of Scientific Research at King Saud University for funding this work through research group no. RG-1441-433 and the research was funded by the Deanship of Scientific Research at the Princess Nourah bint Abdulrahman University through the Fast-track Research Funding Program.

Conflicts of Interest: The authors declare no conflict of interest.

References

1. Dittrich, B.; Wartig, K.-A.; Mülhaupt, R.; Scharfel, B. Flame-retardancy properties of intumescent ammonium poly(phosphate) and mineral filler magnesium hydroxide in combination with graphene. *Polymers* **2014**, *6*, 2875–2895.
2. Bourbigot, S.; Bras, M.L.; Delobel, R. Carbonization mechanisms resulting from intumescence association with the ammonium polyphosphate-pentaerythritol fire retardant system. *Carbon N. Y.* **1993**, *31*, 1219–1230. [[CrossRef](#)]
3. Bourbigot, S.; Le Bras, M.; Delobel, R.; Trémillon, J.M. Synergistic effect of zeolite in an intumescence process: Study of the interactions between the polymer and the additives. *J. Chem. Soc. Faraday Trans.* **1996**, *92*, 3435–3444. [[CrossRef](#)]
4. Bourbigot, S.; Le Bras, M.; Duquesne, S.; Rochery, M. Recent advances for intumescent polymers. *Macromol. Mater. Eng.* **2004**, *289*, 499–511. [[CrossRef](#)]
5. Bourbigot, S.; Patrice, B. 4A zeolite synergistic agent in new flame retardant intumescent formulations of polyethylenic polymers—study of the effect of the constituent monomers. *Polym. Degrad. Stab.* **1996**, *3910*, 275–287. [[CrossRef](#)]
6. Jeyaseelan, C.; Kim, K.H. Effect of precursor ratios on the synthesis of MgAl₂O₄ nanoparticles by a reverse microemulsion method. *J. Ceram. Process. Res.* **2010**, *11*, 96–99.
7. Composites, P.; Aldalbahi, A.; Alotaibi, B.; El-faham, A. Their Effects on Flame Retardancy of polypropylene nanocomposites. *J. Thermoplast. Compos. Mater.* **2020**, 1–11. [[CrossRef](#)]
8. Dai, J.; Li, B. Synthesis, Thermal Degradation, and Flame Retardance of Novel Triazine Ring-Containing Macromolecules for Intumescent Flame Retardant Polypropylene. *J. Appl. Polym. Sci.* **2010**, *116*. [[CrossRef](#)]
9. Delobel, R.; Le Bras, M.; Ouassou, N.; Alistiqsa, F. Thermal Behaviours of Ammonium Polyphosphate-Pentaerythritol and Ammonium Pyrophosphate-Pentaerythritol Intumescent Additives in Polypropylene Formulations. *J. Fire Sci.* **1990**, *8*, 85–108. [[CrossRef](#)]
10. Wang, X.; Wang, Z.; Li, J. Effects of a semi-bio-based triazine derivative on intumescent flame-retardant polypropylene. *Polym. Adv. Technol.* **2019**, *30*, 1259–1268. [[CrossRef](#)]
11. Édelobel, R.; Bourbigot, S.; Le Bras, M.; Schmidt, Y.; Marie Leroy, J. Invariant values of kinetic parameters—Evaluation of fire retardancy application to the PP-APP/PER system. *Makromol. Chemie. Macromol. Symp.* **1993**, *74*, 59–69. [[CrossRef](#)]
12. Feng, C.M.; Zhang, Y.; Lang, D.; Liu, S.W.; Chi, Z.G.; Xu, J.R. Flame retardant mechanism of a novel intumescent flame retardant polypropylene. *Procedia Eng.* **2013**, *52*, 97–104. [[CrossRef](#)]
13. Hu, X.P.; Li, W.Y.; Wang, Y.Z. Synthesis and characterization of a novel nitrogen-containing flame retardant. *J. Appl. Polym. Sci.* **2004**, *94*, 1556–1561. [[CrossRef](#)]
14. Li, G.; Liang, G.; He, T.; Yang, Q.; Song, X. Effects of EG and MoSi₂ on thermal degradation of the intumescent coating. *Polym. Degrad. Stab.* **2007**, *92*. [[CrossRef](#)]
15. Li, Y.; Li, B.; Dai, J.; Jia, H.; Gao, S. Synergistic effects of lanthanum oxide on a novel intumescent flame retardant polypropylene system. *Polym. Degrad. Stab.* **2008**, *93*, 9–16. [[CrossRef](#)]
16. Liu, Y.; Wang, J.S.; Deng, C.L.; Wang, D.Y.; Song, Y.P.; Wang, Y.Z. The synergistic flame-retardant effect of O-MMT on the intumescent flame-retardant PP/CA/APP systems. *Polym. Adv. Technol.* **2010**, *21*, 789–796. [[CrossRef](#)]
17. Lv, P.; Wang, Z.; Hu, K.; Fan, W. Flammability and thermal degradation of flame retarded polypropylene composites containing melamine phosphate and pentaerythritol derivatives. *Polym. Degrad. Stab.* **2005**, *90*, 523–534. [[CrossRef](#)]

18. Wu, Q.; Qu, B. Synergistic effects of silicotungstic acid on intumescent flame-retardant polypropylene. *Polym. Degrad. Stab.* **2001**, *74*, 255–261. [[CrossRef](#)]
19. Nikolic, M.; Lawther, J.M.; Sanadi, A.R. Use of nanofillers in wood coatings: A scientific review. *J. Coat. Technol. Res.* **2015**, *12*, 445–461. [[CrossRef](#)]
20. Patricia, C.; Lovergine, N.; Prete, P. Progress in Crystal Growth and Characterization of Materials: Preface. *Prog. Cryst. Growth Charact. Mater.* **2003**, *47*, 63–64. [[CrossRef](#)]
21. Wang, Q.; Li, W.; Zhang, L.; Zhang, J.; Xiong, W.; Wu, Y.; Song, B.; Mai, Y. Enhanced Flame Retardancy and Mechanical Properties of Intumescent Flame-Retardant Polypropylene with Triazine Derivative-Modified Nano-SiO₂. *Polym. Sci. Ser. B* **2020**. [[CrossRef](#)]
22. Singh, K.; Ohlan, A.; Saini, P.; Dhawan, S.K. Poly (3,4-ethylenedioxythiophene) γ -Fe₂O₃ polymer composite—super paramagnetic behavior and variable range hopping 1D conduction mechanism—synthesis and characterization. *Polym. Adv. Technol.* **2008**, 229–236. [[CrossRef](#)]
23. Tang, Q.; Yang, R.; Song, Y.; He, J. Investigations of flame-retarded thermoplastic poly(imide-urethane)s with intumescent flame retardants. *Ind. Eng. Chem. Res.* **2014**, *53*, 9728–9737. [[CrossRef](#)]
24. Tang, W.; Qian, L.; Chen, Y.; Qiu, Y.; Xu, B. Intumescent flame retardant behavior of charring agents with different aggregation of piperazine/triazine groups in polypropylene. *Polym. Degrad. Stab.* **2019**, *169*. [[CrossRef](#)]
25. Tian, J.; Tian, P.; Ning, G.; Pang, H.; Song, Q.; Cheng, H.; Fang, H. Synthesis of porous MgAl₂O₄ spinel and its superior performance for organic dye adsorption. *RSC Adv.* **2015**, *5*, 5123–5130. [[CrossRef](#)]
26. Wang, G.; Bai, S. Synergistic effect of expandable graphite and melamine phosphate on flame-retardant polystyrene. *J. Appl. Polym. Sci.* **2017**, *134*, 1–9. [[CrossRef](#)]
27. Wang, W.; Wen, P.; Zhan, J.; Hong, N.; Cai, W.; Gui, Z.; Hu, Y. Synthesis of a novel charring agent containing pentaerythritol and triazine structure and its intumescent flame retardant performance for polypropylene. *Polym. Degrad. Stab.* **2017**, *144*, 454–463. [[CrossRef](#)]
28. Emir, H.; Arkiş, E.; Balköse, D.; Ülkü, S. Synergistic effect of natural zeolites on flame retardant additives. *Polym. Degrad. Stab.* **2005**, *89*, 478–483. [[CrossRef](#)]
29. Ravadits, I.; Tóth, A.; Marosi, G.; Márton, A.; Szép, A. Organosilicon surface layer on polyolefins to achieve improved flame retardancy through an oxygen barrier effect. *Polym. Degrad. Stab.* **2001**, *74*, 419–422.
30. Xiao, Z.; Liu, S.; Zhang, Z.; Mai, C.; Xie, Y.; Wang, Q. Fire retardancy of an aqueous, intumescent, and translucent wood varnish based on guanylate phosphate and melamine-urea-formaldehyde resin. *Prog. Org. Coat.* **2018**, *121*, 64–72. [[CrossRef](#)]
31. Xu, B.; Ma, W.; Wu, X.; Qian, L.; Jiang, S. Flame retardancy and thermal behavior of intumescent flame-retardant EVA. *Mater. Res. Express* **2018**, *5*. [[CrossRef](#)]
32. ASTM D2863-13 Standard Test Method for Measuring the Minimum Oxygen Concentration to Support Candle-Like Combustion of Plastics (Oxygen Index); ASTM International: West Conshohocken, PA, USA, 2013.
33. ISO 5660-1 Reaction-to-Fire Tests-Heat Release, Smoke Production and Mass Loss Rate-Part 1: Heat Release Rate (Cone Calorimeter Method); International Standard Organization: Geneva, Switzerland, 2002.
34. Yang, K.; Xu, M.J.; Li, B. Synthesis of N-ethyl triazine-piperazine copolymer and flame retardancy and water resistance of intumescent flame retardant polypropylene. *Polym. Degrad. Stab.* **2013**, *98*, 1397–1406. [[CrossRef](#)]
35. Yang, Z.; Peng, H.; Wang, W.; Liu, T. Crystallization behavior of poly(ϵ -caprolactone)/layered double hydroxide nanocomposites. *J. Appl. Polym. Sci.* **2010**, *116*, 2658–2667. [[CrossRef](#)]
36. Nageswara Rao, T.; Manohra Naidu, T.; Kim, M.S.; Parvatamma, B.; Prashanthi, Y.; Bon Heun, K. Influence of Zinc Oxide Nanoparticles and Char Forming Agent Polymer on Flame Retardancy of Intumescent Flame Retardant Coatings. *Nanomaterials* **2020**, *10*, 42. [[CrossRef](#)] [[PubMed](#)]

